Structure, & Function, ISBN 0-940030-36-5
Volume 1: Nucleic Acids, ISBN 0-940030-37-3
Eds., R.H. Sarma & M.H. Sarma, © Adenine Press 1992

DNA Intercalation: Helix Unwinding and Neighbor-Exclusion

Loren Dean Williams, Martin Egli, Qi Gao† and Alexander Rich
Department of Biology
Massachusetts Institute of Technology
Cambridge, MA USA 02139

Abstract

The molecular basis of DNA unwinding and nearest neighbor-exclusion in intercalated complexes of DNA has remained an area of uncertainty and speculation. We propose a simple model in which DNA helical twist is determined predominantly by a balance of two types of interaction, one that tends to wind the helix, opposed by a second that tends to unwind the helix. Electrostatic repulsion between adjacent phosphate groups tends to wind the helix; winding increases the distances separating adjacent phosphate groups. In opposition are base-base stacking interactions which tend to unwind the helix; unwinding increases the extent of van der Waals contacts between base pairs. Lengthening DNA by inserting an intercalator increases the axial separation of adjacent phosphate groups. The helix unwinds to re-establish B-like distances between adjacent phosphates. Neighbor exclusion arises from helical unwinding; base-base stacking interactions are of greater stability in the vicinity of an intercalator (where the DNA is unwound) than in unperturbed DNA. The binding of a second intercalator adjacent to a first would be relatively unfavorable as this process requires disrupting high-stability base-stacking interactions between unwound base pairs.

Introduction

DNA intercalation, as first proposed by Lerman (1,2), is analogous to insertion of a "false coin" (an intercalator) into a roll of pennies (base pairs). To intercalate in DNA, a planar molecule slides between two base pairs without breaking Watson-Crick hydrogen bonds. Some representative intercalators are shown in Figure 1. Intercalation extends the DNA helix and shifts the base pairs flanking the binding site in opposite directions along the helical axis (Figure 2). Lerman's proposal that planar molecules can intercalate in DNA has been validated by a wealth of physical-chemical data [for reviews see (3-6)] and biological data [for a recent review see (7)].

DNA Unwinding

In the B-conformation of DNA the helical twist is 36°. Each base pair is rotated

† Current address: Analytical Research Department, Bristol-Meyers Squibb Corporation, Wallingford, CT 06492.

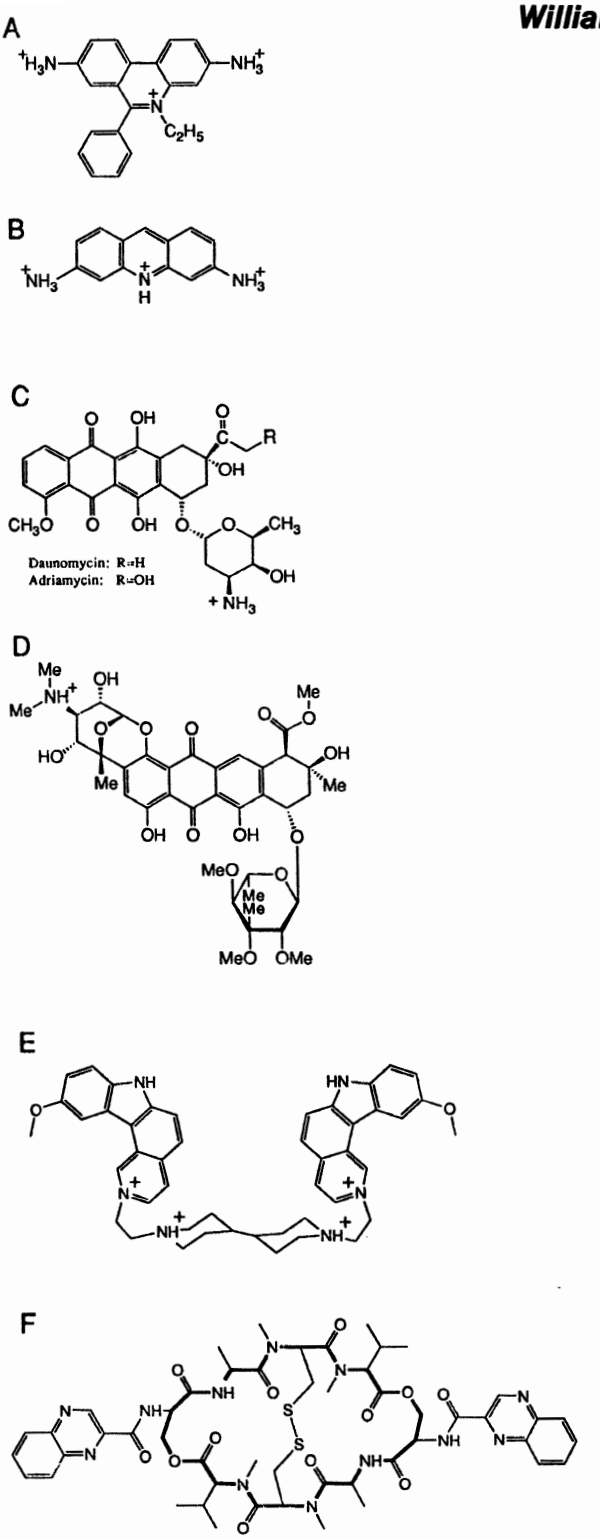

Figure 1: Representative DNA intercalators, (A) ethidium, (B) proflavine, (C) daunomycin, (D) nogalamycin, (E) ditercalinium, and (F) triostin A.

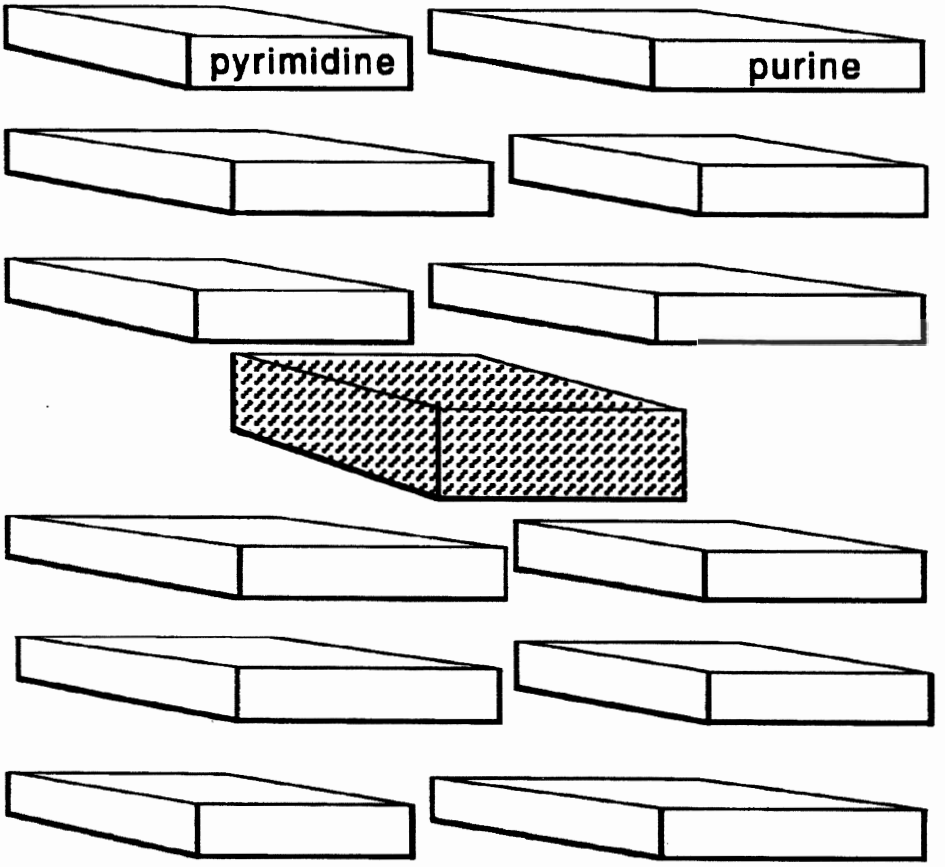

Figure 2: Schematic diagram of DNA intercalation. The intercalator is shaded.

around the helical axis by this amount relative to the preceding base pair. Intercalation invariably decreases the helical twist, unwinding the DNA in the vicinity of the binding site to less than 36° per base pair. The greatest net unwinding by a mono-intercalator is by ethidium with an unwinding angle of 26° per occupied site (8).

A common assumption for rationalizing intercalation-induced DNA unwinding is that it enables the sugar-phosphodiester backbone to span the bound intercalator and still maintain the link between the two flanking base pairs. If so, DNA unwinding provides "slack" in the backbone, and is driven by a length constraint that would otherwise prevent two base pairs from shifting to approximately twice their normal separation along the helical axis. Indeed in a series of DNA and RNA dinucleotide complexes with simple intercalators (such as ethidium or proflavine, Figures 1A and 1B), each small "helix" is unwound at the site of intercalation (9-15). Unwinding at the site of intercalation is a direct prediction of the requirement for slack in the backbone. It was therefore a surprise that in the first complex of an intercalator bound to a larger DNA fragment (daunomycin bound to a DNA hexamer duplex) solved by single-crystal x-ray diffraction (16), the base pairs flanking the intercalator were wound by the normal, B-conformation helical twist of 36°. Yet the DNA in this

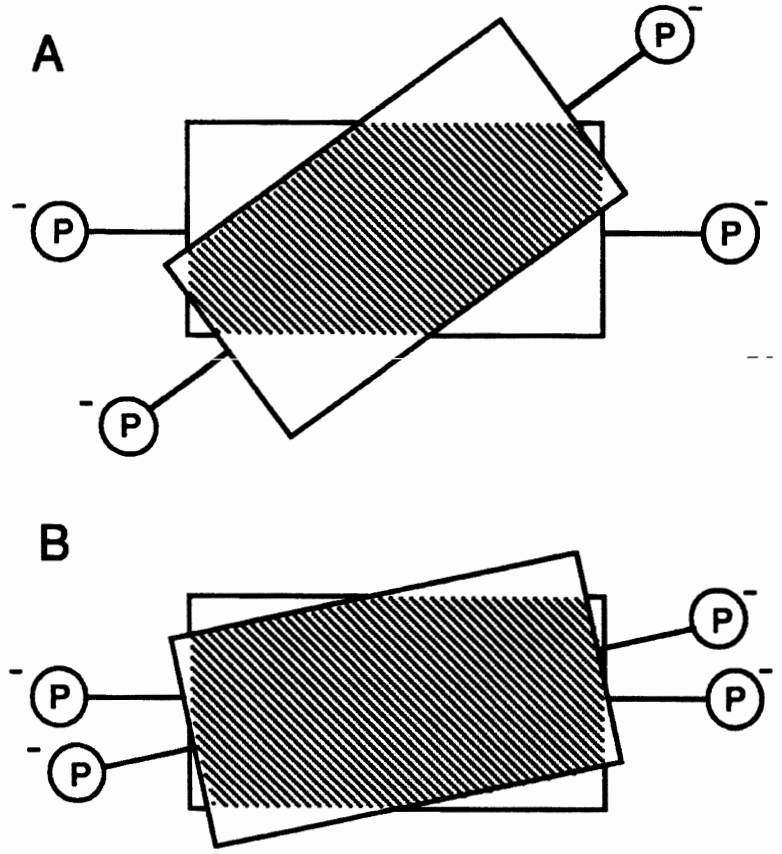

Figure 3: Schematic diagram, viewed down the helical axis, of two residues of DNA with a helical twist of (A) 36° as in B-DNA and (B) 12° to slightly exaggerate the effect commonly observed in intercalated DNA. The area of overlap, indicating the extent of base-base stacking, is shaded. Phosphate groups are represented by encircled P's.

complex was unwound in the region of the helix surrounding the intercalation site. This daunomycin complex and later complexes (17-23) demonstrate that, in the absence of helical unwinding at the intercalation site, the sugar-phosphodiester backbone can easily span the distance between two base pairs flanking an intercalator. It is clear that the helical unwinding invariably induced by DNA intercalation results from some aspect of intercalation other than a requirement for slack in the backbone. Presently the molecular basis for helical unwinding by intercalators in unknown.

Neighbor-Exclusion

The recognition that DNA intercalation obeys the rule of nearest neighbor-exclusion was made by Crothers (24). The rule of neighbor-exclusion states that the two sites directly neighboring an occupied intercalation site must remain unoccupied or, in less absolute terms, intercalation is anti-cooperative at adjacent sites. It was postulated that neighbor-exclusion could arise from stereochemical constraints imposed by the sugar-phosphodiester backbone (10-12). However, single-crystal x-ray structures of

Table I
Distances Between Adjacent Phosphate Groups in DNA-Intercalator Complexes and in B-DNA

Step	Distance (Å)		
	daunomycin-d(CGTACG)		
1 (P2-P3)	6.9		
2 (P3-P4)	7.0		
3 (P4-P5)	6.8		
4 (P5-P6)	6.5		
mean +/− SD	6.8 +/− 0.2		
	daunomycin-d(CGATCG)		
1 (P2-P3)	6.7		
2 (P3-P4)	6.8		
3 (P4-P5)	6.5		
4 (P5-P6)	6.5		
mean +/− SD	6.6 +/− 0.2		
	nogalamycin-d(^{m}CGTsA^{m}CG)		
1 (P2-P3)	6.4		
2 (P3-P4)	6.8		
3 (P4-P5)	6.7		
4 (P5-P6)	6.6		
mean +/− SD	6.6 +/− 0.2		
	ditercalinium-d(CGCG)		
1 (P2-P3)	5.7		
2 (P3-P4)	7.1		
3 (P6-P7)	6.1		
4 (P7-P8)	6.6		
mean +/− SD	6.4 +/− 0.6		
	triostin A-d(GCGTACGC)		
1 (P2-P3)	6.6		
2 (P3-P4)	7.2		
3 (P4-P5)	6.3		
4 (P5-P6)	5.9		
5 (P6-P7)	6.5		
6 (P7-P8)	6.9		
mean +/− SD	6.6 +/− 0.5		
	B-DNA d(CGCGAATTCGCG)[a]		
1 (P2-P3)	6.6	(P14-P15)	6.6
2 (P3-P4)	6.5	(P15-P16)	6.5
3 (P4-P5)	6.8	(P16-P17)	7.1
4 (P5-P6)	6.9	(P17-P18)	6.8
5 (P6-P7)	6.9	(P18-P19)	6.7
6 (P7-P8)	6.3	(P19-P20)	6.7
7 (P8-P9)	6.9	(P20-P21)	6.7
8 (P9-P10)	6.7	(P21-P22)	6.2
9 (P10-P11)	6.6	(P22-P23)	6.6
10 (P11-P12)	7.1	(P23-P24)	6.7
		mean +/− SD	6.7 +/− 0.2

[a] From (28).

intercalated dinucleotides (9-15) and longer DNA fragments (16,17,19-23,25) increasingly demonstrate that the sugar-phosphodiester backbone is flexible and polymorphic. Modelling studies have shown that stereochemically reasonable structures which violate neighbor-exclusion can be constructed (26). Presently the molecular basis for neighbor-exclusion, like that of DNA unwinding, is unknown.

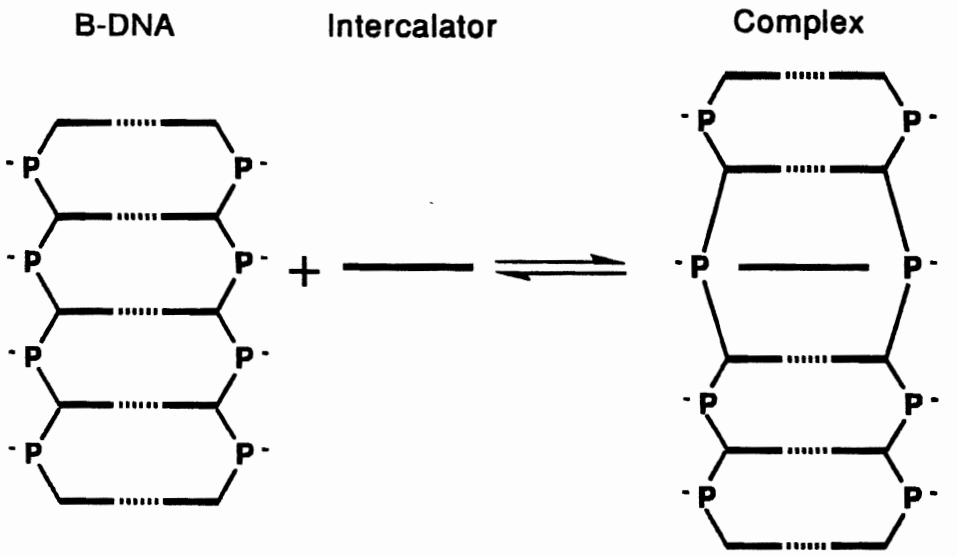

Figure 4: Schematic diagram, viewed perpendicular to the helical axis, of the non-covalent reaction between DNA and an intercalator. The intercalator is represented by a long thick line, bases by short thick lines, Watson-Crick hydrogen bonds by dashed lines. The deoxyribo-phosphodiester backbone is represented by thin lines interrupted by P's.

Relationships between intercalation, helical unwinding and neighbor-exclusion remain unclear. The absence of a plausible molecular basis for neighbor-exclusion and helical unwinding derives primarily from a lack of understanding of helical twist in general. It is probably impossible to decipher the causes of intercalator-induced DNA unwinding and neighbor-exclusion until the molecular basis for the helical twist of unperturbed DNA is understood. Here we provide a self-consistent and reasonable molecular basis for DNA helical twist, intercalator-induced unwinding and neighbor-exclusion.

A Model

We propose that DNA helical twist is determined predominantly by a balance of two types of interaction, one that tends to wind the helix, opposed by a second that tends to unwind the helix. In our model, electrostatic repulsion between adjacent phosphate groups tends to wind the helix. As shown schematically in Figure 3, decreasing the helical twist of the DNA helix decreases the separation between adjacent phosphate groups. In B-DNA, which displays a helical twist of 36°, the distance between adjacent phosphate groups averages 6.7 Å (Table I) (27,28). This distance appears to be highly constrained in crystal structures of B-DNA, never falling below 6.2 Å. This lack of variability is consistent with substantial electrostatic repulsion at shorter distances.

In our model, helical winding by electrostatic repulsion is opposed by base-base stacking interactions, which tend to unwind the helix. Stacking interactions are the principle contributor to thermodynamic stability of duplex DNA (29). We propose that base-base stacking interactions tend to unwind the helix because, as shown

schematically in Figure 3, unwinding the helix increases the extent of base-base van der Waals contacts. Increasing van der Waals contacts between base pairs increases the contribution of stacking to thermodynamic stability of the duplex. Thus helical twist of DNA is achieved by a balance of electrostatic repulsion between adjacent phosphate groups against base-base stacking interactions.

Although intercalation lengthens DNA, increasing the axial separation of adjacent phosphate groups (shown in Figure 4), x-ray crystallographic structures of intercalated DNA demonstrate that the distances between adjacent phosphate groups do not increase. These distances remain approximately equal to those of B-DNA (Table I). The average distance between adjacent phosphate groups is 6.8 Å in the daunomycin-d(CGTACG) complex, 6.6 Å in the daunomycin-d(CGATCG) complex and 6.6 Å in the nogalamycin-d(^{m}CGTsA^{m}CG) complex (see Figure 1C for daunomycin and Figure 1D for nogalamycin). Even in bis-intercalated complexes, which display greater helical distortions than mono-intercalated complexes, the average distance between adjacent phosphate groups remains nearly the same as observed in B-DNA. The average distance between adjacent phosphate groups is 6.4 Å in the ditercalinium-$[d(CGCG)]_2$ complex (25) and 6.6 Å in the triostin A-d(GCGTACGC) complex (17) (see Figure 1E for ditercalinium and Figure 1F for triostin). In addition, the distances between adjacent phosphate groups are relatively uniform within each complex and are not greater at the site of intercalation than elsewhere. This invariance of the distances between adjacent phosphate groups supports the importance of adjacent-phosphate electrostatic repulsion in DNA winding and in DNA conformation in general.

In intercalated complexes, B-like distances are maintained between adjacent phosphate groups because unwinding compensates for lengthening. DNA lengthening increases the axial projection of the distance separating adjacent phosphate groups (Figure 4). DNA unwinding decreases the base pair plane projection of the distance separating adjacent phosphate groups (Figure 3). When an intercalator binds, the DNA both lengthens and unwinds with the result that the distances separating adjacent phosphate groups remain unchanged. We suggest the lowest energy conformation should exhibit the greatest degree of stacking (i.e., the greatest helical unwinding) allowed by repulsion between adjacent phosphate groups. Thus the proposal that helical twist is determined predominantly by a balance of destabilizing electrostatic interactions versus stabilizing stacking interactions is consistent with intercalator-induced DNA unwinding. Any increase in the length of DNA is expected to unwind the helix, increasing the extent of stacking interactions between base pairs.

This model accounts for neighbor-exclusion, providing a reasonable molecular basis for anti-cooperative binding at adjacent sites. In the vicinity of an intercalator (where the DNA is unwound and base-base overlap is more extensive), stacking interactions would contribute more to duplex stability than in unperturbed DNA. At a site of intercalation, base-base stacking interactions must be disrupted. The binding of a second intercalator adjacent to a first would then require disrupting high-stability stacking interactions between unwound base pairs. The relative free energy of binding of the second intercalator would be offset by the amount required to disrupt these high-stability stacking interactions. Thus for neighboring intercalators, the relative free energy of binding of the second would be less than for the first.

It merits mention that models of DNA complexes are notoriously error-prone. There are few examples of x-ray structures of DNA complexes that have been even grossly predicted *de novo* by such techniques as molecular mechanics calculations. It is difficult to predict even such elementary characteristics as whether a given functional group will reside in the major or in the minor groove [for example see (30)]. As noted by Harvey, in molecular mechanics modelling, difficulties produced by the high formal charge of DNA and the extensive solvent accessible surface (31) are countered by physically unrealistic approaches such as rendering dielectric terms distant-dependent, fixing positions of phosphate groups or substantially reducing their charges. However, repulsive interactions between phosphate groups are surely a primary determinant of nucleic acid conformation and in principle should be explicitly incorporated in a physically realistic way. The model described here, unlike those used for molecular mechanics, attempts only to describe gross structural features (such as helical twist), and incorporates adjacent phosphate repulsion as a primary determinant of nucleic acid structure. Our model provides a self-consistent and reasonable molecular basis for relating DNA helical twist, intercalator-induced unwinding and neighbor-exclusion.

Although distances between adjacent phosphate groups remain nearly constant in the intercalated complexes that have been crystallized thus far, other characteristics of DNA unwinding are polymorphic. The crystal structures demonstrate that the net unwinding of DNA by an intercalator can partition within a helix in several ways. The DNA commonly does not unwind directly at the site of intercalation but unwinds in the surrounding region. Although we propose that stacking interactions in general tend to unwind DNA, the location and extent of unwinding in intercalated DNA would be modulated by the structure of the intercalator. As described in detail below, we believe that it is possible to understand and predict how a given intercalator will bind to and distort DNA based on the three-dimensional shape of the intercalator.

Parallel and Perpendicular Intercalators

Intercalators can be conceptually placed into two classes. The first class of intercalators, termed here "parallel", contains molecules which lack bulky substituents along their long axis. The parallel class of intercalators is composed of molecules such as ethidium, proflavine, and bis-intercalators such as ditercalinium (Figure 1). A space filling representation of ethidium (Figure 5A and 5B) shows an example of the three-dimensional shape of a parallel intercalator. The second class of intercalators, termed here "perpendicular", contains molecules which contain bulky substituents at one or both ends of their long axis. The perpendicular class of intercalators is composed of molecules such as daunomycin and nogalamycin (Figure 1). A space filling representation of nogalamycin (Figure 5C and 5D) shows an example of the three-dimensional shape of a perpendicular intercalator. DNA complexes of both parallel (9-15,25) and perpendicular (16-23) intercalators have been solved by x-ray crystallography. This classification scheme is based on our observation that in x-ray crystal structures, intercalators lacking bulky substituents along their long axis bind to DNA oriented with their long axis nearly parallel to those of the flanking base pairs. Intercalators with bulky substituents along their long axis bind to DNA oriented with their long axis nearly perpendicular to the average of those of the flanking base pairs.

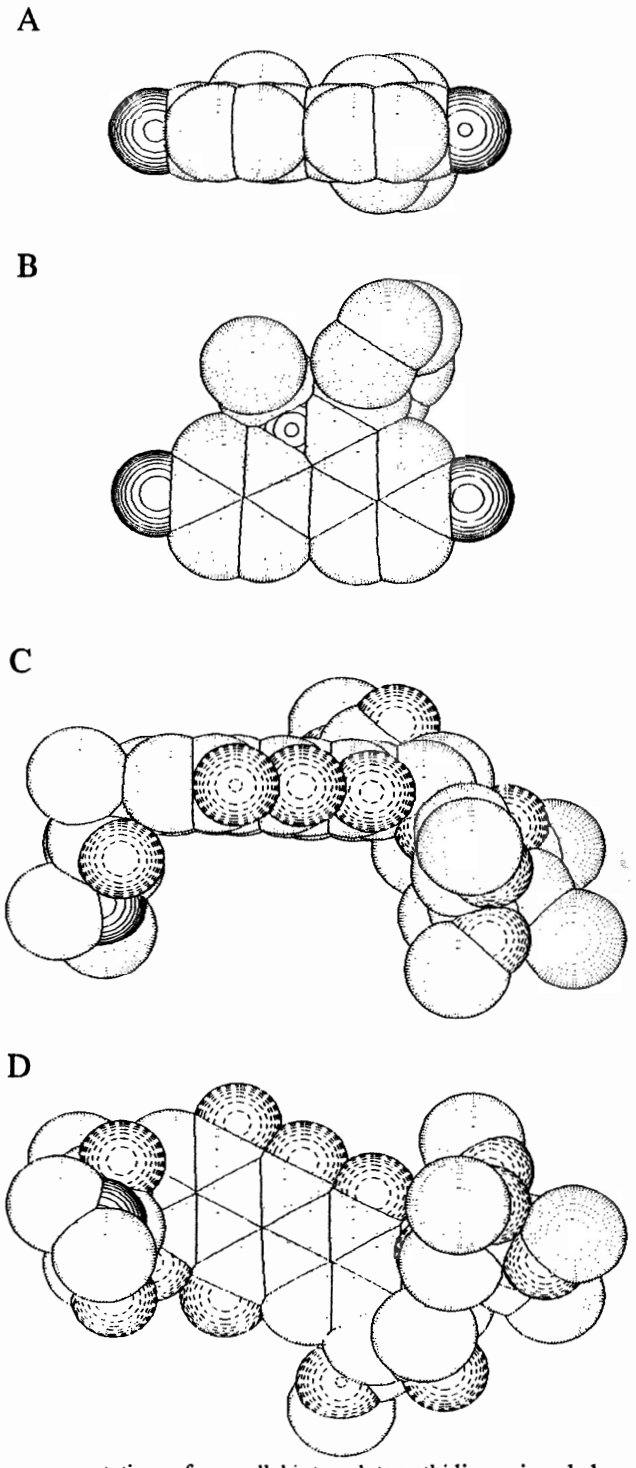

Figure 5.: Space filling representations of a parallel intercalator, ethidium, viewed along (A) the edge and (B) the perpendicular to the plane of the intercalator, and a perpendicular intercalator, nogalamycin, viewed along the (C) edge and (D) perpendicular to the plane of the intercalator. Carbon atoms are marked by concentric dots, oxygen atoms by concentric dashes, and nitrogen atoms by concentric lines.

A

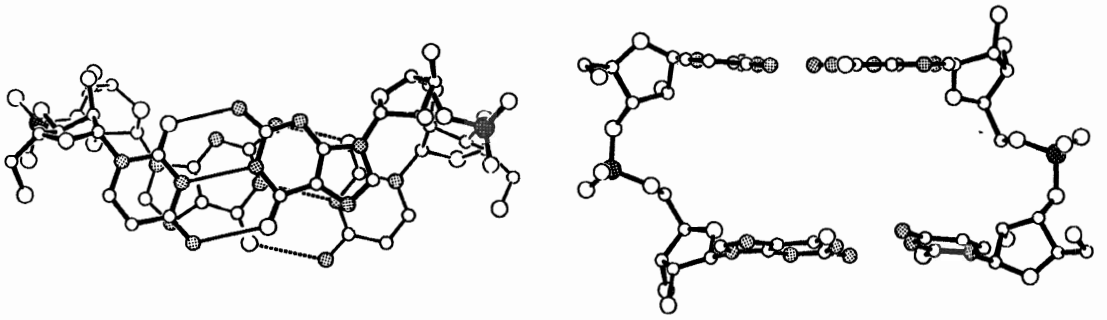

C(1) - - - G(2)

G(2) - - - C(1)

B

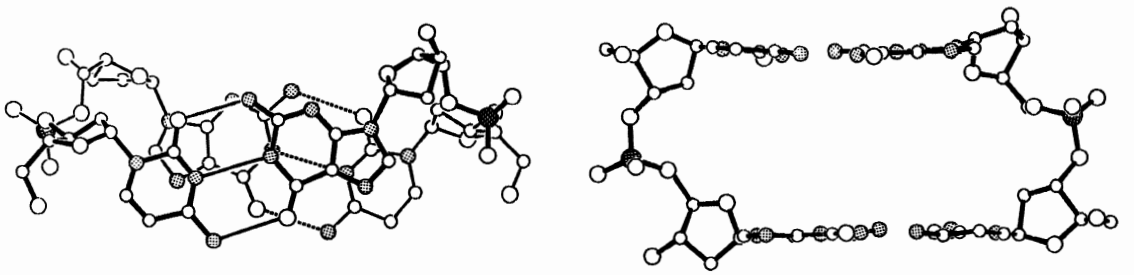

C(1) - - - G(2)

G(2) - - - C(1)

Figure 6: Complexes between (A) r(CG) plus ethidium (15) and (B) d(CG) plus proflavine (14). The intercalators have been omitted. The views are (left) along the perpendicular of the best plane of the top base pair and (right) along the best plane of the top base pair, looking into the major groove. Atom types are coded according to size with P > O > N > C. Nitrogen atoms are stippled in grey, and phosphorus atoms are stippled in black. On the left the top base pair is drawn with thick lines, and the bottom base pair is drawn with thin lines, the hydrogen bonds in the top base pairs are solid lines and hydrogen bonds in the bottom base pairs are dashed lines. On the right, hydrogen bonds have been omitted.

There are three features that distinguish DNA complexes with parallel intercalators from those with perpendicular intercalators.

(a) In parallel type complexes, as described above, the long axis of the intercalator is oriented nearly parallel to the long axes of the flanking base pairs while in perpendicular complexes the long axis of the intercalator is oriented nearly perpendicular to the

A

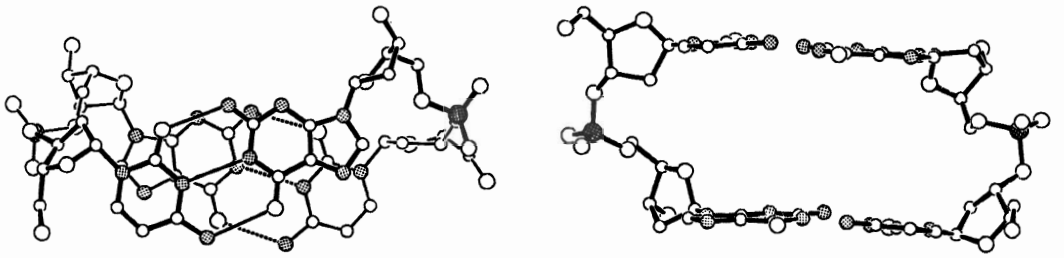

C(1) - - - G(8)

G(2) - - - C(7)

B

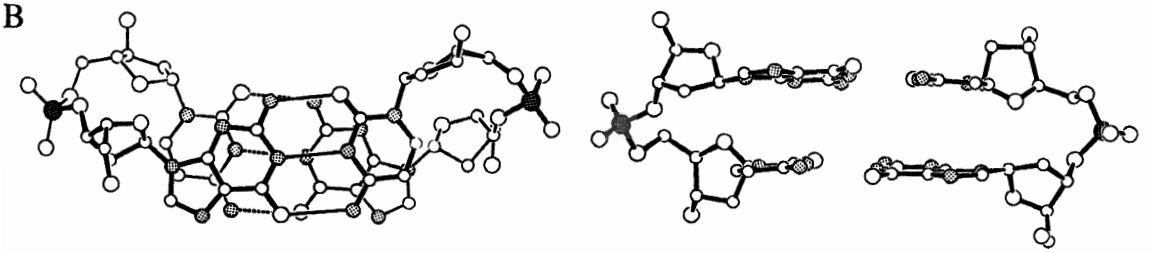

G(2) - - - C(7)

C(3) - - - G(6)

C

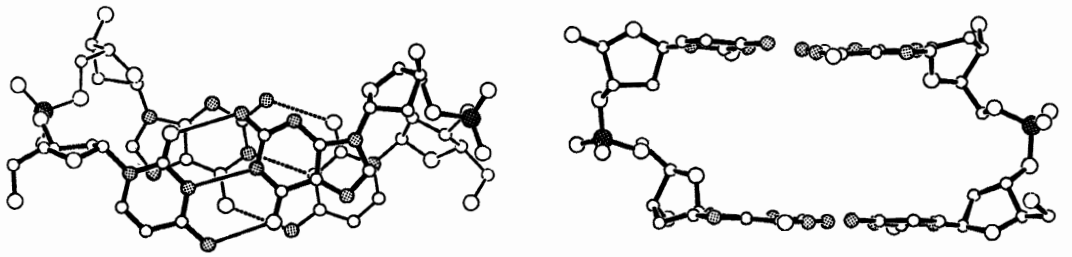

C(3) - - - G(6)

G(4) - - - C(5)

Figure 7: The DNA from the the ditercalinium-d(CGCG) complex. The ditercalinium molecule has been omitted. The views are (left) along the perpendicular of the best plane of the top base pair and (right) along the best plane of the top base pair, looking into the major groove. (A) The terminal C(1)-G(2) · C(7)-G(8) step, (B) the G(2)-C(3) · G(6)-C(7) step, and (C) the C(3)-G(4) · C(5)-G(6) step. Atom types are coded according to the convention of Figure 6.

A

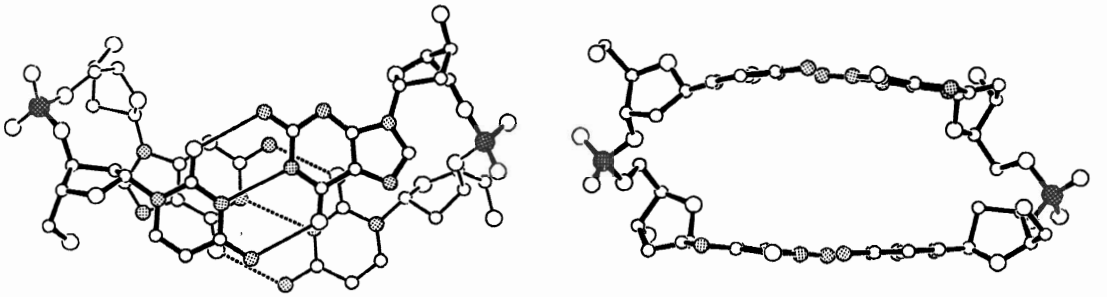

C(1) - - -G(12)

G(2) - - -C(11)

B

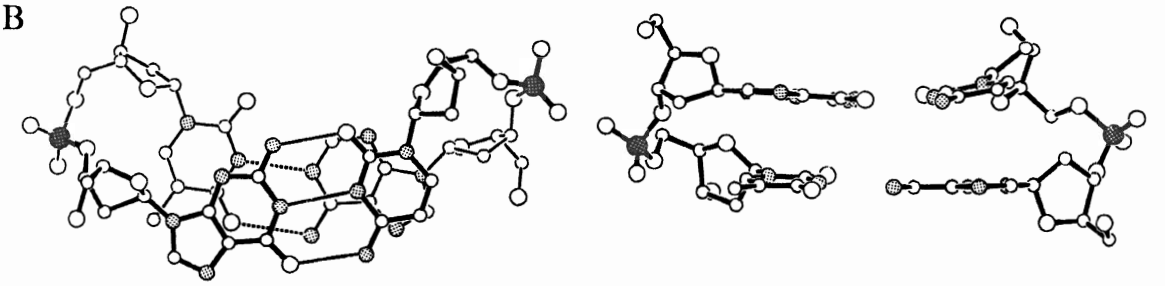

G(2) - - -C(11)

T(3) - - -A(10)

C

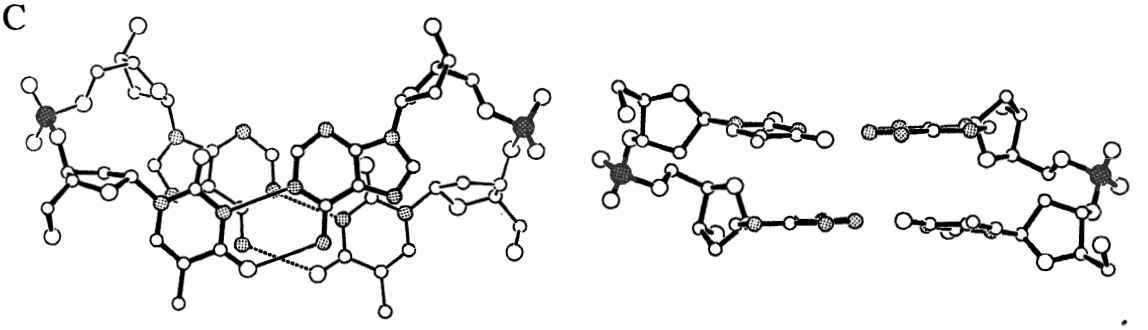

T(3) - - -A(10)

A(4) - - -T(9)

Figure 8: The DNA from the daunomycin-d(CGTACG) complex. The daunomycin molecule has been omitted. The views are (left) along the perpendicular of the best plane of the top base pair and (right) along the best plane of the top base pair, looking into the major groove. (A) The terminal C(1)-G(2)·C(11)-G(12) step, (B) the G(2)-T3)·A(10)-C(11) step, and (C) the T(3)-A(4)·T(9)-A(10) step. The two base pairs in the third step are related by a crystallographic 2-fold rotation. Atom types are coded according to the convention of Figure 6.

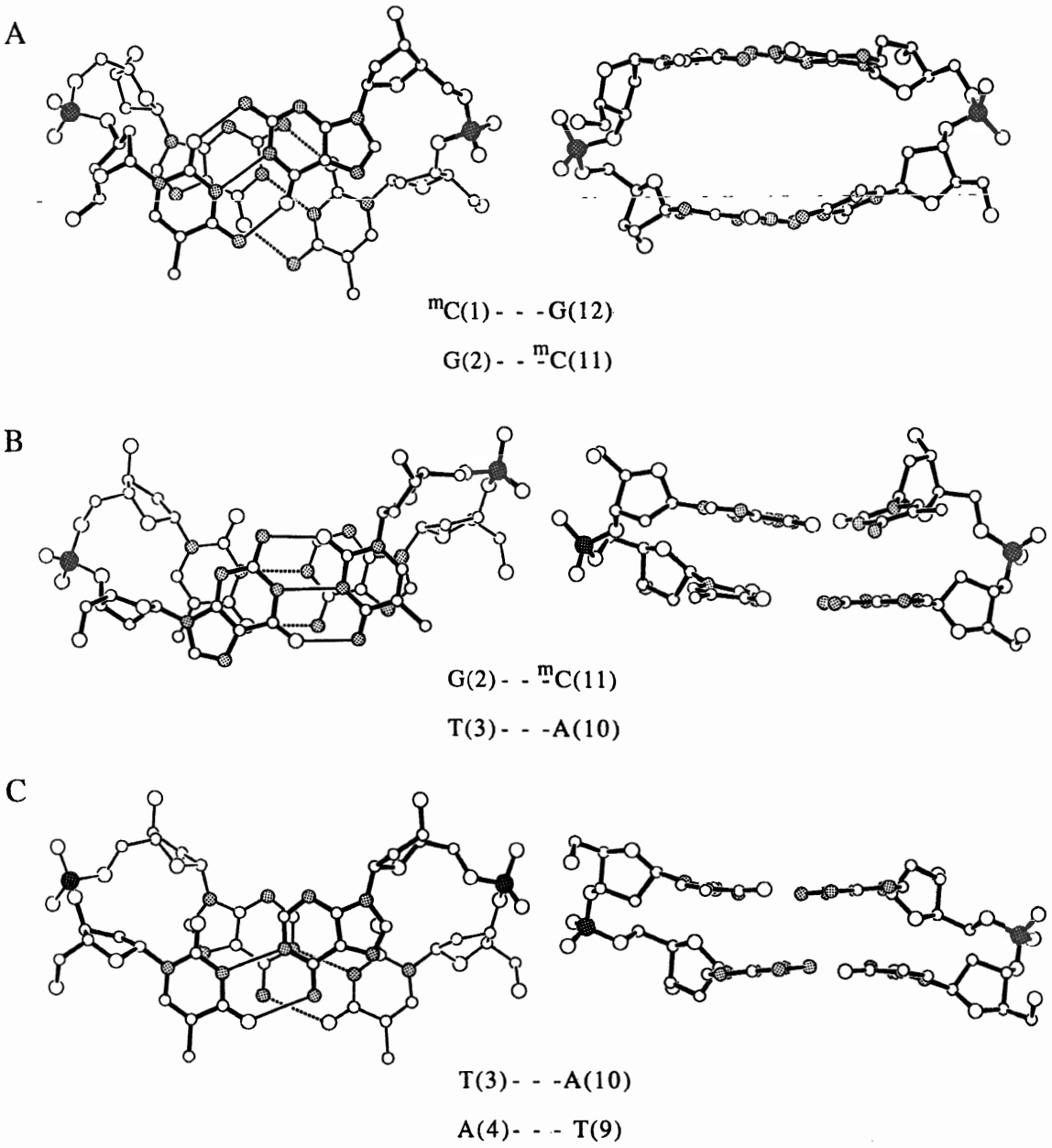

Figure 9: The DNA from the nogalamycin-d(^{m}CGTsA^{m}CG) complex. The nogalamycin molecule has been omitted. The views are (left) along the perpendicular of the best plane of the top base pair and (right) along the best plane of the top base pair, looking into the major groove. (A) The terminal ^{m}C(1)-G(2) · ^{m}C(11)-G(12) step, (B) the G(2)-T(3) · A(10)-^{m}C(11) step, and (C) the T(3)-A(4) · T(9)-A(10) step. The two base pairs in the third step are related by a crystallographic 2-fold rotation. The two base pairs in the third step are related by a crystallographic 2-fold rotation. Atom types are coded according to the convention of Figure 6.

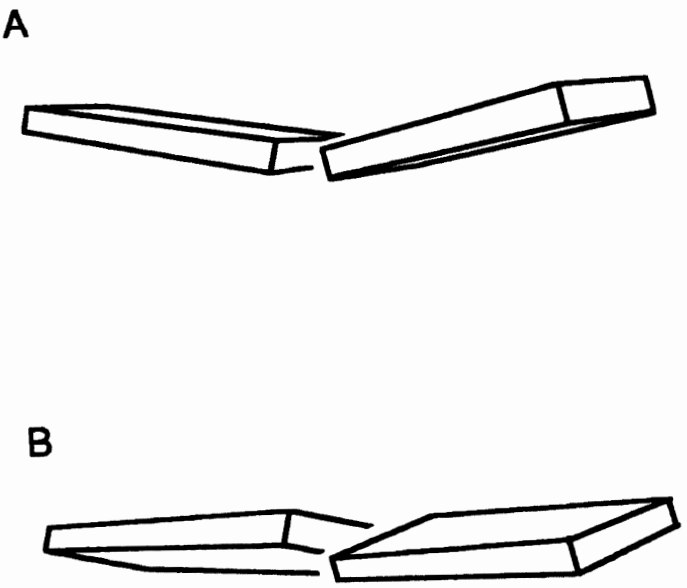

Figure 10: Schematic diagram of base pairs that are (A) buckled and (B) propeller twisted.

long axes of the flanking base pairs. The parallel orientation provides greater van der Waals stabilization but is sterically inaccessible to perpendicular type intercalators.

(b) In parallel type complexes, DNA unwinds at the site of intercalation (left sides of Figures 6A, 6B, 7A and 7C) while in perpendicular complexes the DNA does not (left sides of Figures 8A and 9A). However, in perpendicular complexes the DNA unwinds in the region surrounding the site of intercalation (left sides of Figures 8B, 8C, 9B and 9C). Unwinding the DNA at the site of intercalation increases van der Waals stabilization in the parallel complexes by aligning the long axis of the intercalator and the two flanking base pairs. In perpendicular complexes no increase in van der Waals contacts would be achieved by unwinding at the intercalation step. The observed unwinding at the site of intercalation in parallel complexes, and the lack thereof in perpendicular complexes, supports the importance of stacking interactions in maintaining nucleic acid helical twist.

(c) In parallel complexes the base pairs flanking the intercalator are relatively planar (right sides of Figures 6 and 7) while in perpendicular complexes the base pairs "curve" (right sides of Figures 8 and 9). The Watson-Crick hydrogen bonds of a base pair form a relatively flexible joint linking the two rigid bases. The joint allows the base pair to curve by buckling and propeller twisting (Figure 10) (32). In parallel complexes the planarity of the base pairs actually increases relative to B-DNA [as noted previously (33)]. However, in perpendicular complexes, the DNA base pairs curve to wrap around an intercalator and maximize van der Waals contacts. In each crystal structure of a perpendicular complex the first base pair buckles in the negative direction while the second step buckles in the positive direction (Table II). The buckle of the first step varies from $-8.1°$ in a daunomycin-d(CGTACG) complex to $-10.9°$ in a nogalamycin-d(^{m}CGTsA^{m}CG) complex. The buckle of the second step varies

Table II
Selected Helical Parameters of DNA-Intercalator Complexes (Degrees)

Step	Helical Twist	Buckle	Propeller Twist
ethidium-r(CG)			
1*	26[a]	− 0.5[b]	2.9[b]
2	- -	− 1.6	5.4
proflavine-d(CG)			
1*	28[a]	4.3[b]	12.3[b]
2	- -	4.3	12.3
daunomycin-d(CGTACG)			
1*	35.0[c]	− 8.1[c]	−0.6[c]
2	30.9	16.4	−2.0
3	34.5	3.7	−6.8
daunomycin-d(CGATCG)			
1*	35.4[c]	− 9.4[c]	−1.4[c]
2	31.6	16.2	−0.1
3	32.0	6.3	−3.1
nogalamycin-d(^{m}CGTsA^{m}CG)			
1*	35.6[c]	−10.9[c]	−4.4[c]
2	24.8	26.2	−1.6
3	39.4	8.5	−4.3
ditercalinium-d(CGCG)			
1*	18.8[d]	− 0.3[c]	8.4[c]
2	28.6	5.4	1.9
3*	24.3	1.1	8.7
4	- -	− 5.1	−5.0

* intercalation step.
[a] estimated.
[b] from (33).
[c] calculated with the program "Newhelix" (32).
[d] calculated with the program "Curves" by Lavery and Sklenar.

from 16.2° in the daunomycin-d(CGTACG) complex to 26.2° in the nogalamycin-d(^{m}CGTsA^{m}CG) complex. The curvature of the base pairs which flank a perpendicular intercalator create a cavity within the DNA conforming roughly to the shape of the intercalator. This approximation of the shape of the cavity to that of the intercalator results in the extensive van der Waals contacts between the base pairs and the intercalator. Thus van der Waals interactions are the most likely cause for the curvature uniformly observed in the base pairs flanking perpendicular intercalators.

A schematic diagram of a hypothetical complex formed by an intercalator bound in the parallel orientation to B-DNA is shown in Figure 11A. The van der Waals contacts between the flanking base pairs and the intercalator increase when the helix unwinds (Figure 11B) to a state observed in the crystal structures.

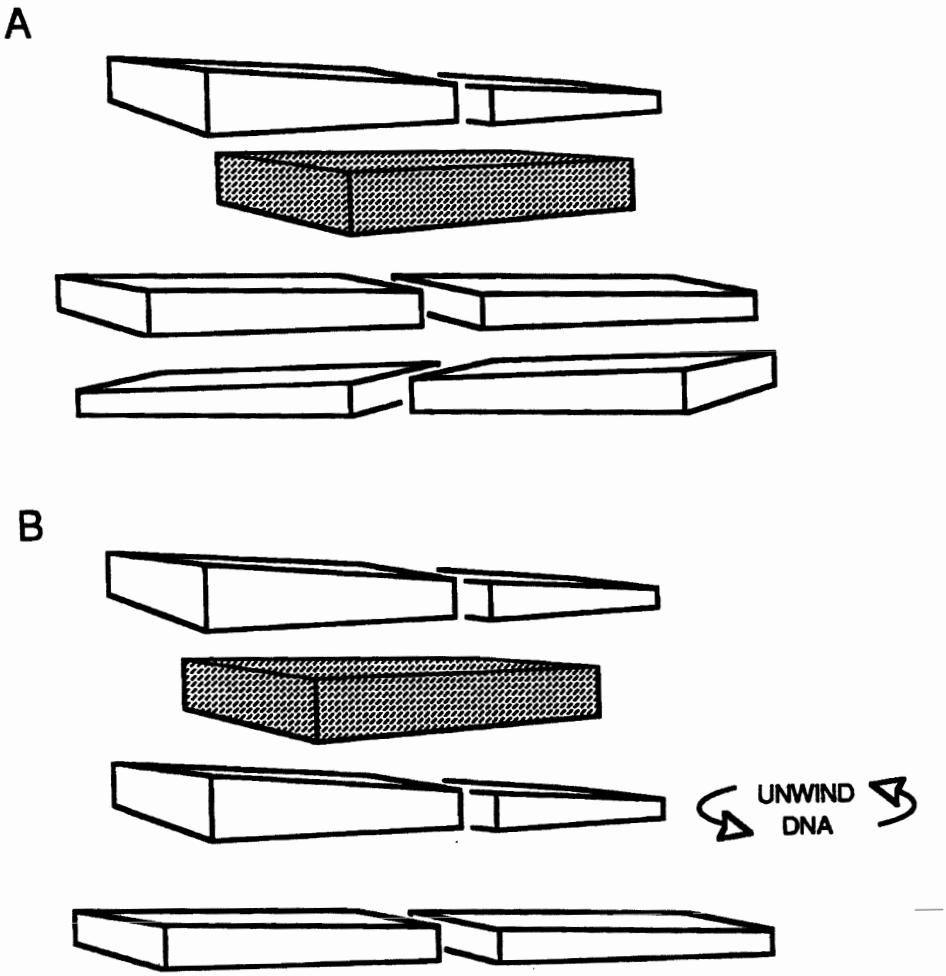

Figure 11: A schematic diagram of three base pairs flanking a parallel intercalator, which is shaded, in (A) canonical B-DNA, and (B) underwound DNA.

A schematic diagram of a hypothetical complex formed by an intercalator bound in the perpendicular orientation to B-DNA is shown in Figure 12A. The van der Waals contact between the intercalator and the flanking base pairs increase when the base pairs curve at the flexible joint provided by the hydrogen bonds (Figure 12B). This curvature of the base pairs provides a molecular mechanism for transmission of distortions along the helix. When a base pair immediately flanking a perpendicular intercalator curves, the van der Waals contact with the next base pair would decrease if that base pair remained planar (in canonical B-conformation) as shown in Figure 12B. The crystal structures demonstrate that there are two conformational adjustments by which the next base pair maintains sufficient van der Waals contacts with the first. One adjustment is propeller twist (Figure 12C). In crystal structures of intercalated perpendicular complexes, the propeller twist of the second base pair from the intercalator varies from -3.1 to $-6.8°$ (Table II), always in the direction that increases stacking interactions with the

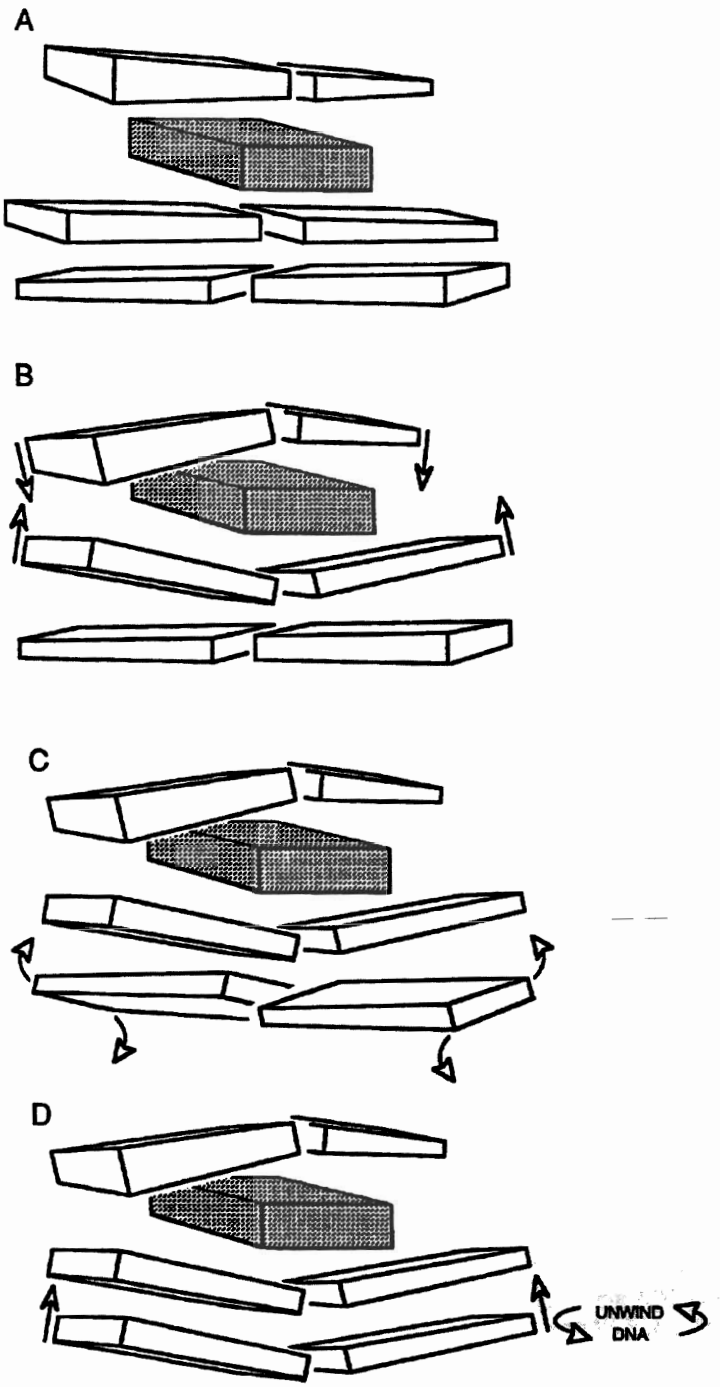

Figure 12: A schematic diagram of three base pairs and a perpendicular intercalator, which is shaded, (A) in a canonical B-DNA, (B) with the base pairs flanking the intercalator buckled to wrap around the intercalator, (C) with the second base pair from the intercalator propeller twisted, and (D) with the second base pair from the intercalator buckled and the helix unwound.

first base pair. Although propeller twist improves van der Waals contacts between these two base pairs, a second conformational adjustment of the second base pair from the intercalator also contributes. This adjustment is buckling coupled with helical unwinding to give a conformation shown schematically in Figure 12D. Buckling plus unwinding effectively places adjacent bases on parallel planes, again maximizing van der Waals contacts. As observed in the crystal structures, perpendicular complexes do not unwind DNA at the site of intercalation but at neighboring sites (Table II). One might expect that in a modulated fashion, the third base pair from the intercalator in turn might lose planarity and unwind and so forth, transmitting helical distortions induced by an intercalator along the DNA helix. There is currently no crystal structural data available on these more distant effects.

Summary

We propose that helical twist of DNA is determined predominantly by a balance of two types of interactions. Electrostatic repulsion between adjacent phosphate groups tends to wind the helix and base-base stacking interactions tend to unwind the helix. This model successfully accounts for helical twist of B-DNA, and DNA unwinding and neighbor-exclusion in intercalated complexes.

To understand and predict helical distortion by intercalators, we have classified intercalating molecules based on their three-dimensional shapes. We predict that in DNA complexes with parallel intercalators, the DNA is unwound primarily at the site of intercalation and helical distortions (such as buckling and propeller twisting) are localized primarily in the vicinity of the intercalator. Alternatively, in complexes with perpendicular intercalators, the DNA is unwound in more dispersed regions surrounding the intercalator and helical distortions are transmitted for relatively greater distances from the site of intercalation along the helical axis. More specifically, this model predicts that anticooperativity of intercalation should extend for greater distances from the site of intercalation of a perpendicular intercalator than of a parallel intercalator. Since helical distortions are likely to be important in function of DNA binding therapeutic agents, this model shows promise for understanding relationships between structure and activity.

Acknowledgements

We thank Dr. Nassim Usman for helpful discussions. This research was supported by grants from the National Institutes of Health, the American Cancer Society, the National Science Foundation, the Office of Naval Research and the National Aeronautics and Space Administration. L.D.W. acknowledges fellowship support by the National Institutes of Health and the Medical Foundation Inc., Boston, MA. M.E. acknowledges fellowship support by the Geigy-Jubiläums-Stiftung. The coordinates of the dinucleotide complexes were obtained from the Cambridge Structural Database.

References and Footnotes

1. L.S. Lerman, *J. Mol. Biol. 3*, 18 (1961).
2. L.S. Lerman, *J. Cell Comp. Physiol. 64 (suppl. 1)*, 1 (1964).
3. M.J. Waring, *Ann. Rev. Biochem. 50*, 159 (1981).

4. H.M. Berman and P.R. Young, *Ann. Rev. Biophys. Bioeng. 10*, 87 (1981).
5. S. Neidle and Z. Abraham, *CRC Rev. Biochem. 17*, 73 (1985).
6. S. Neidle, L.H. Pearl and J.V. Skelly, *Biochem. J. 243*, 1 (1987).
7. W.A. Denny, *Anti-cancer Drug Design 4*, 241 (1989).
8. J.C. Wang, *J. Mol. Biol. 89*, 783 (1970).
9. S. Neidle, A. Achari, G.L. Taylor, H.M. Berman, H.L. Carrell, J.P. Glusker and W.C. Stallings, *Nature (London) 269*, 304 (1977).
10. C. Tsai, S.C. Jain and H.M. Sobell, *J. Mol. Biol. 114*, 301 (1977).
11. S.C. Jain, C. Tsai and H.M. Sobell, *J. Mol. Biol. 114*, 315 (1977).
12. H.M. Sobell, C. Tsai, S.C. Jain and S.G. Gilbert, *J. Mol. Biol. 114*, 333 (1977).
13. H.M. Berman, W. Stallings, H.L. Carrell, J.P. Glusker, S. Neidle, G. Taylor and A. Achari, *Biopolymers 18*, 2405 (1979).
14. H.-S. Shieh, H.M. Berman, M. Dabrow and S. Neidle, *Nucleic Acid Res. 8*, 85 (1980).
15. S.C. Jain and H.M. Sobell, *J. Biomol. Struct. Dynamics 1*, 1179 (1984).
16. G.J. Quigley, A.H.-J. Wang, G. Ughetto, G.A. van der Marel, J.H. van Boom and A. Rich, *Proc. Natl. Acad. Sci. USA 77*, 7204 (1980).
17. G.J. Quigley, G. Ughetto, G.A. van der Marel, J.H. van Boom, A.H.-J. Wang and A. Rich, *Science 232*, 1255 (1986).
18. M.H. Moore, W.N. Hunter, B. Langlois d'Estaintot and O. Kennard, *J. Mol. Biol. 206*, 693 (1989).
19. C.A. Frederick, L.D. Williams, G. Ughetto, G.A. van der Marel, J.H. van Boom, A. Rich and A.H.-J. Wang, *Biochem. 29*, 2538 (1990).
20. L.D. Williams, M. Egli, Q. Gao, P. Bash, G.A. van der Marel, J.H. van Boom, A. Rich and C.A. Frederick, *Proc. Natl. Acad. Sci. USA 87*, 2225 (1990).
21. L.D. Williams, C.A. Frederick, G. Ughetto and A. Rich, *Nucleic Acids Res. 18*, 5533 (1990).
22. L.D. Williams, M. Egli, G. Ughetto, G.A. van der Marel, J.H. van Boom, G.J. Quigley, A.H.-J. Wang, A. Rich and C.A. Frederick, *J. Mol. Biol. 215*, 313 (1990).
23. M. Egli, L.D. Williams, C.A. Frederick and A. Rich, *Biochem. 30*, 1364 (1991).
24. D.M. Crothers, *Biopolymers 6*, 575 (1968).
25. Q. Gao, L.D. Williams, M. Egli, D. Rabinovich, S.-H. Chen, G.J. Quigley and A. Rich, *Proc. Natl. Acad. Sci. USA 88*, 2422 (1991).
26. S.N. Rao and P.A. Kollman, *Proc. Natl. Acad. Sci. USA 84*, 5735 (1987).
27. R. Wing, H. Drew, T. Takano, C. Broka, S. Takana, K. Itakura and R.E. Dickerson, *Nature (London) 287*, 755 (1980).
28. W. Saenger, *Principles of Nucleic Acid Structure*, (Springer-Verlag, New York) (1984).
29. H. DeVoe and J.I. Tinoco, *J. Mol. Biol. 4*, 500 (1962).
30. D.A. Collier, S. Neidle and J.R. Brown, *Biochem. Pharmacol. 33*, 2877 (1984).
31. S.C. Harvey, *Proteins: Structure, Function and Genetics 5*, 78 (1989).
32. R.E. Dickerson, *Nucleic Acids Res. 17*, 1797 (1989).
33. C.C. Wilson, *Nucleic Acids Res. 16*, 5229 (1988).